Environ. Sci. Technol. **2002**, *36,* 2338−2344

Distribution and Reactivity of O_2-Reducing Components in Sediments from a Layered Aquifer

NIELS HARTOG,*,† JASPER GRIFFIOEN,‡ AND CORNELIS H. VAN DER WEIJDEN†

Department of Geochemistry, Faculty of Earth Sciences, Utrecht University, P.O. Box 80021, 3508 TA Utrecht, Utrecht, The Netherlands

The redox status of subsurface aqueous systems is controlled by the reactivity of solid redox-sensitive species and by the inflow of such species dissolved in groundwater. The reactivity toward molecular oxygen (O_2) of solid reductants present in three particle size fractions of sediments from a pristine aquifer was characterized during 54 days. The stoichiometric relationships between carbon dioxide (CO_2) production and O_2 consumption was used in combination with sulfate production to discriminate between the contributions of sedimentary organic matter (0−87%), pyrite (6−100%), and siderite (0−43%) as the dominant reductants. The observed simultaneous oxidation of these reductants indicates that they are reactive on the same time scales. The measured reduction capacity (8−84 μmol O_2/g) ranged from 8 to 42% of the total reduction capacity present as pyrite and organic carbon in the total sediment fraction (<2 mm). Fine fractions (<63 μm) were 10−250 times more reactive than their corresponding total fractions. Oxygen consumption rates decreased continuously during carbonate buffered conditions, due to a decreasing reactivity of reductants. Acidification accelerated pyrite oxidation but impeded SOM respiration. Our findings indicate that the geological history of aquifer sediments affects the amounts of organic matter, pyrite and siderite present, while environmental conditions, such as pH and microbial activity, are important in controlling the reactivity of these reductants. These controls should be considered when assessing the natural reduction activity of aquifer sediments in either natural or polluted systems.

Introduction

The natural potential of aquifer sediments to reduce oxidants is of general interest in groundwater chemistry. For instance, due to excessive fertilization and manuring extensive leaching of nitrate from agricultural fields occurs (*1*−*4*), and the fate of this nitrate is controlled by the reactivity of the reductants present in the subsurface (*5*−*11*). Degradation of organic contaminants is also controlled by the redox status of the contaminated groundwater (*12*−*15*). The anaerobic degradation of benzene is of prime interest (*16, 17*), as is the reductive dechlorination of chlorinated hydrocarbons by reactive reductants (*18, 19*). The injection of oxidants such as oxygen, nitrate, or sulfate may enhance the breakdown of monoaromatics (*16, 17, 20*), but an important drawback for stimulated in-situ bioremediation in contaminated aquifers is the competition of natural reductants for injected oxidants (*21, 22*).

Understanding the reactivity of reductants present in aquifer sediments thus deserves attention. Common reductants in aquifer sediments are sedimentary organic matter (SOM) and pyrite (FeS_2), but ferrous iron in silicates, siderite ($FeCO_3$), and vivianite as well as exchangeable ferrous iron are potentially reactive reductants too (*23*). Pyrite and siderite are commonly found in close association with organic matter due to redox processes occurring during or after deposition (*24*). Therefore, a relationship between the reduction capacity and the diagenetic history of sediment can be expected. Furthermore, fine-grained sediments are generally richer in organic material and associated reduced mineral phases (*8, 25*), and higher total reduction capacities for aquifer sediments with a larger fine fraction have been suggested (*26*). Recently, Christensen et al. discussed studies on the reduction capacity of aquifer sediments (*27*). The TRC of sediments can be calculated if all relevant reduced components are recognized, and their quantification is sufficiently accurate. However, this approach yields a maximum potential, since it does not account for the reactivities of these components.

In this study, we focus on the reduction reactivity of pristine aquifer sediments by measuring the O_2 consumption during incubations. Together with the overall change in aqueous composition, we use the stoichiometry between the O_2 consumption and CO_2 production to identify the ongoing oxidation reactions. Our objectives were (1) to determine the relative contribution of the identified reductants to the reduction activity, (2) to assess the difference in the reduction capacity of different grain size fractions, and (3) to evaluate the impact of geological stratification on the reduction activity within a layered single aquifer unit that consists of three geological units.

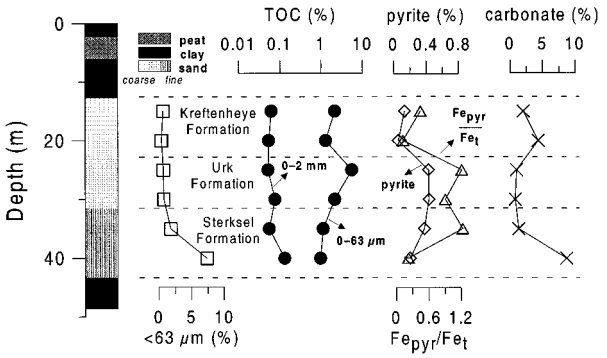

FIGURE 1. Geological description of the sediments and geochemical characteristics of the total fractions (0−2 mm) used. Depth is referenced in meters below surface level. A log scale was used for the TOC (%) to show also the data for the fine fraction (<63 μm).

Materials and Methods

Sample Collection and Processing. Six core samples were taken from a borehole in a sandy aquifer at the drinking water production site "De Steeg" near Langerak, The Netherlands. This aquifer was selected since it contains three distinct geological formations, covering a range from coarse to fine sands (Figure 1). Furthermore, this location is proposed as a site for recharge through riverbank infiltration, which

* Corresponding author phone: (+31) 30 253 4991; fax: (+31) 30 253 5302; e-mail: nhartog@geo.uu.nl.
† Utrecht University.
‡ TNO Netherlands Institute of Applied Geosciences.

10.1021/es015681s CCC: $22.00
Published on Web 05/03/2002

TABLE 1. Oxidation Reactions of Considered Reduced Components with Molecular Oxygen

		CO_2/O_2	ΔG_r^0 [a]
a	$FeCO_3 + {}^1/_4O_2 + 1{}^1/_2H_2O \rightarrow Fe(OH)_3 + CO_2$	4	−468
b	$C_9H_{10}O_5$ [b] $+ 9O_2 \rightarrow 9CO_2 + 5H_2O$	1	−433[c]
c	$FeS_2 + 3{}^3/_4O_2 + 1{}^1/_2H_2O + 2CaCO_3 \rightarrow Fe(OH)_3 + 2Ca^{2+} + 2SO_4^{2-} + 2CO_2$	8/15	−507
d	$FeS_2 + 3{}^3/_4O_2 + 3{}^1/_2H_2O \rightarrow Fe(OH)_3 + 2SO_4^{2-} + 4H^+$	0	−477
	And with Ferrous Iron on Exchange Site X_2		
e	$Fe\text{-}X_2 + {}^1/_4O_2 + CaCO_3 + 1{}^1/_2H_2O \rightarrow Ca\text{-}X_2 + Fe(OH)_3 + CO_2$	4	

[a] ΔG_r^0 values calculated from ref *33*. [b] Syringate ($C_9H_{10}O_5$) is used as a model compound for SOM (*34*). [c] Value for acetic acid.

would result in a gradual oxidation of this aquifer that is currently under iron(III)-reducing conditions. Sediment cores were collected anaerobically at depth using Akkerman sampling tubes. The tubes were stored under a nitrogen atmosphere at 8 °C directly after field collection. The tubes were opened in a N_2-filled glovebox in which sediment samples were prepared for further study. By wet sieving, three particle size fractions were separated: 0−2000 μm (total fraction), 0−63 μm (fine fraction), and 63−2000 μm (coarse fraction). The remaining fraction containing particles larger than 2 mm was not further analyzed.

Geology. Holocene clays and peat confine the top of the aquifer; Early Pleistocene clays confine its bottom. The Kreftenheye Formation contains coarse fluvio-glacial sands, deposited during the Late Pleistocene. The Urk Formation consists of medium sized Middle Pleistocene fluvial sands, deposited in a perimarine environment. The Sterksel Formation consists of fine fluvial sands from the Early Pleistocene (Figure 1).

Sediment Incubations. Samples were incubated under dark conditions. Twenty-five milliliters of vitamin and trace element solution were added in order to prevent inhibition due to nutrient limitation. Sample weight ranged from a few grams for the fine fraction to 100 g for the total fraction. The reaction chambers (100-mL bottle, Duran) were connected to the closed circuit of a respirometer (Micro-Oxymax, Columbus Instruments). Water-saturated gases were used to prevent evaporation in the reaction chambers. Oxygen ($p_{O_2} = 10^{-0.69\pm0.004}$ atm) and carbon dioxide ($p_{CO_2} = 10^{-3.3\pm0.11}$ atm) levels in the headspaces were kept at atmospheric conditions at 25 °C (± 1 °C). The O_2 consumption and CO_2 production were measured every 3 h for 54 days, using an infrared sensor and an oxygen battery (fuel cell), respectively. The reaction chambers were shaken (100 rpm) to ensure a well-mixed chemical system and prevent oxygen transfer limitations.

Analytical Procedures. Directly after incubation pH was measured with a standard pH meter (Orion), and alkalinity was determined by acid titration. Dissolved cations and sulfate were analyzed using ICP-AES (Perkin-Elmer ICP-optima 3000). X-ray fluorescence (XARL8410) was used to determine total iron (Fe_t) and total sulfur (S_t) contents of the sediments. Total organic carbon (TOC) was measured on freeze-dried sediments using a method adapted from Jakobsen et al. (*28*), in which we used 2.6 M HCl to remove inorganic carbon. TOC was determined as the sum of two fractions: acid dissolvable organic carbon (ADOC), and the residual organic carbon (NADOC). ADOC content was measured as dissolved organic carbon in the acid solution (TOC-500, Shimadzu), while NADOC content was determined in the remaining solid sample by oxidation (NA1500 NCS, Carlo Erba). Pyrite contents were determined by HNO_3 extraction, and total carbonate contents were determined as weight loss after acid digestion. Thermogravimetry is often used to assess the amounts of carbonates, but no good method yet exists to quantify low siderite concentrations in aquifer sediments (*27*). We tested a combination of thermogravimetry (TGA) and differential thermal analysis (TG-DTA92, Setaram).

Total Reduction Capacity. The TRC was expressed in mmol O_2/g.sed to enable direct comparison with the experimental data and was calculated using analyzed contents of total organic carbon [TOC], pyrite [FeS_2] according to eq 1.

$$TRC = 3{}^3/_4[FeS_2] + 1[TOC]\ (\text{mmol } O_2/\text{g.sed}) \quad (1)$$

Here, $3{}^3/_4$ and 1 refer to the stoichiometric coefficients of pyrite and SOM oxidation, respectively (Table 1). When present, siderite contributes to the TRC as well but was left out of the calculation, because of its qualitative determination (see Results and Discussion section).

Geochemical Modeling. PHREEQC-2 (*29*) was used to model the chemical evolution in the batch chambers, using the O_2 consumption over time as an input and the CO_2 production as an output constraint. PHREEQC-2 was also used to determine saturation indices (SI), where SI is equal to the logarithmic value of the ratio between the ion activity product (IAP) and the solubility product (K_s) for the mineral phases considered.

Results and Discussion

Reductants Present in the Aquifer Sediments. Significant amounts of pyrite and organic matter were present in all sediment samples (Figure 1). In the Urk Formation, where the highest pyrite contents (up to 4350 ppm) were found, pyritic iron (Fe_{pyr}) accounted for most of the total iron (Fe_t) (Figure 1) Furthermore, the molar ratio between Fe_t and total sulfur contents (Fe_t/S_t) was close to 0.5. This indicates that other iron containing minerals were insignificant. High Fe_t and low S_t concentrations were present in the deepest sediment taken from the Sterksel Formation. With 22% of Fe_t present in pyrite, an additional source of iron, such as iron hydroxides, detrital phyllosilicates, or siderite must be present. The weight loss during heating (TGA) confirmed the presence of calcite but not of siderite. However, using differential thermal analysis (DTA), two distinct endothermic peaks between 500 and 600 °C and 700−850 °C were observed (see Figure S1, Supporting Information), that are in agreement with both the disintegration temperatures of siderite and calcite from literature data (*30*−*32*) and the standards used. These results point to a siderite content of less than 1% in this carbonate-rich sediment. Thus, organic matter, pyrite, and siderite are the main potentially reactive reductants present in the aquifer sediments studied. However, predicting which reductant is most prone to oxidation is difficult because these species have comparable energy yields for their oxidation (*33*), while their oxidation mechanisms are distinctly different (Table 1).

Identification of Important Oxidation Reactions. Theoretical CO_2/O_2 Ratios for Oxidation Reactions. The ratio of CO_2 production to O_2 consumption is commonly used as respiratory quotient for the organic substrate. The molar CO_2/O_2 ratio for the complete oxidation of organic matter varies

with chemical composition from 1.0 for the oxidation of carbohydrates ($C_nH_{2n}O_n$) to 0.8 for the oxidation of a more reduced organic compound as benzene (C_6H_6). The composition of SOM in the studied sediments, as derived from pyrolysis-GC-MS analyses, shows a predominantly aromatic signature derived from lignin. Syringate ($C_9H_{10}O_5$) has a chemical structure similar to methoxylated aromatic compounds that make up lignin (*34*). Therefore we use syringate as a model compound for SOM, as shown in reaction b (Table 1).

While CO_2 production is inherent to the oxidation of organic matter, CO_2 production during pyrite or Fe(II) oxidation depends on the presence of reactive carbonates.

Under carbonate equilibrium conditions, the theoretical molar CO_2/O_2 ratio is distinctly different during pyrite oxidation, as shown in reaction c, than during the sole oxidation of ferrous iron, as shown in reaction a. In the absence of reactive carbonates, pyrite oxidation will not result in CO_2 production, and the CO_2/O_2 ratio will therefore be zero, as shown in reaction d. Pyrite, SOM, and siderite are commonly found in other sedimentary aquifers, but reactive reductants, such as $MnCO_3$ ($CO_2/O_2 = 2$) or FeS ($CO_2/O_2 = 0.44$), can be assessed using the same approach. Since the resulting CO_2/O_2 ratio of co-oxidizing reductants is not unique, constraints are needed to calculate their relative contributions. Here, sulfate is used to constrain the importance of pyrite oxidation.

Calculating the Relative Importance of Reductants. The relative contribution of pyrite ($f_{pyr-buf}$) to the total oxygen consumption under carbonate buffered and unbuffered ($f_{pyr-unbuf}$) conditions can be calculated from the total sulfate production (eq 3). Then, the relative contribution of siderite (f_{sid}), SOM (f_{SOM}) to the total O_2 consumption can be calculated using the cumulative CO_2/O_2 ratios (eq 4).

$$f_{pyr} + f_{SOM} + f_{sid} = 1 \tag{2}$$

$$f_{pyr} = f_{pyr-buf} + f_{pyr-unbuf} = \frac{3\,^3/_4 \sum SO_4}{2 \sum O_2} \tag{3}$$

$$\frac{\sum CO_2}{\sum O_2} = 4f_{sid} + f_{SOM} + \frac{2}{3\,^3/_4} f_{pyr-buf} \tag{4}$$

Here, $\sum O_2$, $\sum CO_2$, and $\sum SO_4$ are the total amounts of O_2 consumed, CO_2 produced, and sulfate produced, respectively. Equation 4 is valid if carbonate equilibrium and undersaturation for gypsum ($CaSO_4 \cdot 2H_2O$) are maintained during the incubation (chemistry of supernatants section).

When pyrite oxidation proceeds unbuffered by carbonate dissolution, $f_{pyr-unbuf}$ is calculated using eq 5, where $\sum O_2{}^*$ is the total amount of oxygen consumption that was unaccompanied by CO_2 release.

$$f_{pyr-unbuf} = \frac{\sum O_2{}^*}{\sum O_2} \tag{5}$$

Observed Processes during Sediment Incubations. The ratios between total CO_2 produced and total O_2 consumed during the incubation experiments ranged between 0.05 and 2.7 (Figure 2). These are within the range of CO_2/O_2 stoichiometries for the oxidation of pyrite, organic matter, and siderite (Table 1) but do not correspond to the stoichiometric oxidation of one of these main reductants. Therefore the observed CO_2/O_2 ratios must be the result of their combined oxidation (eq 2).

Total Fraction Incubations. As shown in Figure 2, SOM oxidation is predominant in the Kreftenheye Formation, as

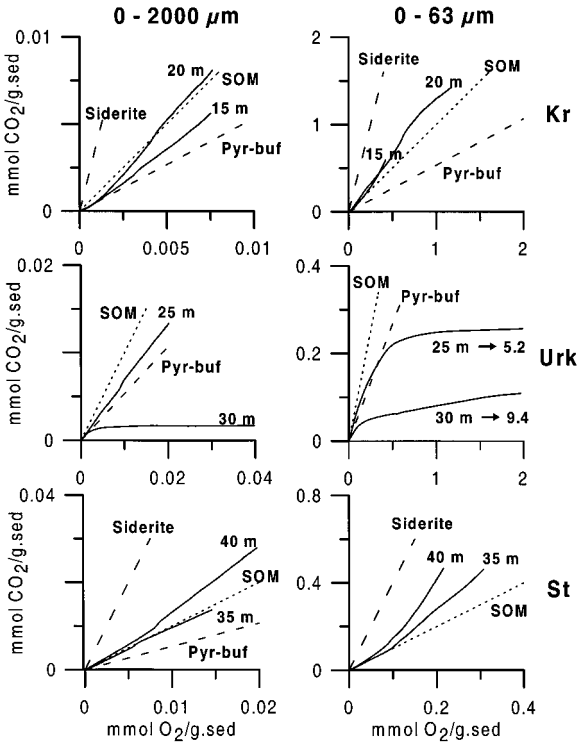

FIGURE 2. Cumulative O_2 consumption and CO_2 production during the total and fine sediment fraction incubations (54 days) are represented by solid lines. Kr, Urk, and St denote Kreftenheye, Urk, and Sterksel Formation, respectively. The fine fractions of the Urk Formation were plotted up to 2 mmol O_2/g.sed (total consumption indicated with arrow). Stoichiometric lines (dashed) are shown for siderite, SOM and pyrite oxidation under carbonate buffered conditions. Note the different scales for the axes.

based on the theoretical oxidation stoichiometry (Table 1). Pyrite oxidation is the foremost process in the Urk Formation. Initially, the 30-m incubation shows CO_2 production and O_2 consumption according to the stoichiometric oxidation of pyrite oxidation under carbonate buffered conditions and subsequently O_2 consumption without CO_2 production. This indicates that the buffering capacity is limited and that the oxidation of organic matter or siderite is insignificant during the acidification, caused by unbuffered pyrite oxidation. Sediment incubations of the Sterksel Formation (35 and 40 m) show the oxidation of pyrite, SOM, and siderite. Especially, the deepest sediment shows elevated (>1) CO_2/O_2 ratios and thus the largest contribution by siderite oxidation. This is in line with the detection of siderite in this sediment. The CO_2/O_2 ratios changed little during the total fraction incubations that were carbonate buffered, indicating that the reductants were oxidized concurrently.

Fine Fraction Incubations. The oxidation of SOM is most pronounced in the fine fraction incubations of the Kreftenheye Formation (Figure 2), indicating that diagenetically formed reductants were absent or less reactive. The fine fractions of the Sterksel Formation show elevated CO_2/O_2 ratios toward the end of the incubations (Figure 2), indicating an increasing importance of siderite oxidation. Although the oxidation of exchangeable ferrous iron, as shown in reaction e, would result in an identical CO_2/O_2 ratio, the estimated release of ferrous iron from cation-exchange sites in these fine fractions was insignificant compared with the total observed O_2 consumption. Moreover, it would be expected to proceed early in the experiments, since desorption (*35*, *36*) and oxidation of aqueous ferrous iron at circumneutral pH (*37*) are both almost instantaneous. The CO_2/O_2 ratios of the fine fraction incubations of the Urk Formation (Figure

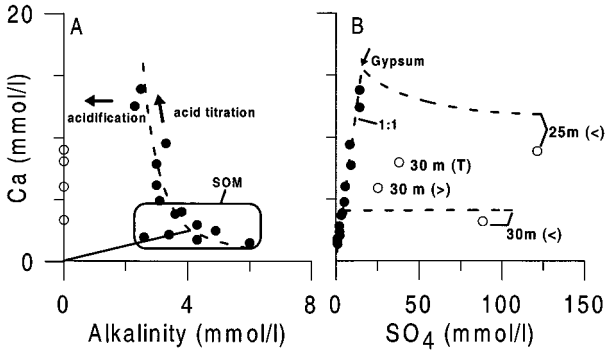

FIGURE 3. Final concentrations in the supernatants of (A) calcium and alkalinity and (B) calcium and sulfate. Filled and open circles represent buffered and acidified samples, respectively. The solid line in (A) represents calcite equilibrium for increasing CO_2-pressure, the rectangle encompasses samples that show over 70% SOM oxidation and that are therefore less influenced by acid titration. The arrow in (B) indicates the onset of gypsum saturation and the dashed lines describe the modeling results. Depth (m) is shown for the acidified total (T), coarse (>) and fine (<) fractions.

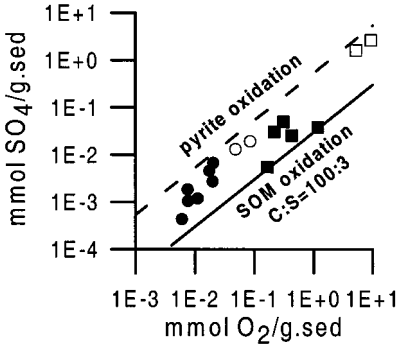

FIGURE 4. O_2 consumption and total sulfate production for total and coarse (both circles) and fine (squares) fractions. Carbonate buffered and acidified incubations are represented by filled and open symbols, respectively. Lines refer to stoichiometric oxidation of pyrite and SOM. Note the logarithmic scales.

2) initially show buffered pyrite oxidation followed within a week by pyrite oxidation unbuffered by carbonate dissolution. Even though the fine fractions of the Urk and Sterksel Formation are relatively enriched in TOC (Figure 1), the diagenetically formed reductants in the fine fractions are more reactive than SOM.

Coarse Fraction Incubations. The coarse fractions were less reactive (55−86%) compared with the total fractions. The carbonate buffered coarse fractions show a greater contribution (52−86%) by SOM oxidation compared with the corresponding total and fine fractions. However, SOM oxidation was insignificant during the incubation of the coarse fraction from 30 m depth, which acidified due to the pyrite oxidation that proceeded largely (75%) unbuffered by carbonates.

Chemistry of Supernatants after Incubation. Final pHs, alkalinities, and calcium concentrations of the supernatants were all in agreement with carbonate equilibrium, except for the incubations that showed unbuffered pyrite oxidation, which acidified to pH values of 1.6−2.5 (Figure 3a). The relatively high CO_2 production rates in combination with the low equilibrium concentration of CO_2 ($10^{-3.5}$ atm) caused a build-up of CO_2 ($10^{-1.7}$ atm) in the supernatants. However, this was less than 1% of the total CO_2 production in all incubations. Therefore, overall CO_2/O_2 ratios were not significantly affected.

The interpretations based on CO_2/O_2 ratios are in keeping with the chemical composition of the supernatants after incubation. Incubations that dominantly showed buffered pyrite oxidation have higher calcium concentrations (up to 15 mmol/L) and lower alkalinities compared with those expected from calcite dissolution in equilibrium with the CO_2 pressure in the headspaces. Especially, final calcium and sulfate concentrations in the supernatant of the carbonate buffered incubations were highly correlated along the theoretical stoichiometry for pyrite oxidation but were still undersaturated with respect to gypsum (Figure 3b). This indicates that H^+ production during pyrite oxidation was the main drive for the dissolution of sedimentary calcite. Total sulfate production was highest for samples that showed a pyrite oxidation CO_2/O_2 stoichiometry (Urk Formation). In these samples the total sulfate production was also related to the total O_2 consumption along the pyrite oxidation stoichiometry (Figure 4). The incubated fractions of the Kreftenheye Formation from 20 m depth show CO_2/O_2 ratios that are closest to SOM oxidation. If sulfate in these experiments is the product of SOM oxidation only, then the degree of sulfurization (S/C) of the oxidized SOM (0.03) is high compared with those of organic matter (0.006−0.03) in freshwater lake sediments (*38*). Although it is not possible to distinguish between an organic or pyritic source of the sulfate, it is clear that pyrite oxidation contributes very little to the observed total O_2 consumption in these incubations.

In the four samples where pyrite oxidation resulted in acidic supernatants, final sulfate concentrations could only account for half of the total O_2 consumption. Since CO_2 production ceased in these incubations (Figure 2), the additional oxidation of SOM or siderite oxidation cannot account for this discrepancy. Therefore, the precipitation of sulfate-containing solids controlled the final sulfate concentrations in these samples. This hypothesis was tested by modeling the pyrite oxidation in the two fine fractions of the Urk Formation with PHREEQC-2 (*29*). We used the total amount of O_2 consumption and CO_2 production as a constraint for the total amount of pyrite oxidation and the total amount of reactive carbonate buffer, respectively. A model containing only calcite and pyrite and K-feldspar (as a source of potassium) was used. Results (Figure 3b) indicated the likely precipitation of K-jarosite ($KAl_3(OH)_6(SO_4)_2$) as well as gypsum during the incubation of the fine fraction from 30 and 25 m depth, respectively. Considering the limited number of input constraints, the modeled pH and final calcium and sulfate concentrations agree very well with the measured values in the supernatants.

Reactivity of Reduced Components. Our results show that pyrite, SOM, and siderite were oxidized simultaneously during our sediment incubations (Table 2). To assess their separate reactivities, we will next consider experiments in which one reductant was dominantly important.

Sedimentary Organic Matter. In the fine (Figure 5a) and coarse (Figure 5b) fraction from 20 m depth, SOM accounted for 85% and 86% of the total O_2 consumption. Both incubations show continuously decreasing O_2 consumption rates. Decreasing respiration rates are often observed (e.g. ref *39*) and are attributed to an increasing stability of the residual organic compounds (*40, 41*). In comparison with the coarse fractions, the importance of SOM oxidation was less important in the fine fractions than the oxidation of pyrite and siderite. This can be due to a decreased reactivity of SOM in the fine fractions as a result of physical protection through sorption and complexation of SOM by clay minerals (*42*) or to a higher degree of mineralization of the original SOM during to the formation of reduced secondary minerals, like pyrite and siderite, during diagenesis (*40*). Even though the acid hydrolysis of SOM during unbuffered pyrite oxidation resulted in final DOC concentrations up to 87 mg/L, SOM oxidation was not observed. This is probably due to the inhibition of microbial respiration under acid conditions (*43*).

TABLE 2. TRC Values of the Total Fractions, as Calculated from SOM and Pyrite Contents and Final MRC Values for the Total and Fine Fractions[a]

depth (m)	TRC (μmol O_2/g)	mRC (μmol O_2/g)	pH	SO_4 (μmol/g)	CO_2/O_2 (molar)	oxidation reactions (%) (a)	(b)	(c)	(d)
Total Fractions (0−2 mm)									
15	93	8	7.2	1.8	0.75		54	46	
20	62	8	7.5	1.0	1.06	6	68	26	
25	176	20	6.3	6.7	0.66		38	62	
30	199	84	2.1	19.1	0.02			9	91
35	164	15	6.8		0.94		87	13	
40	172	20	7.1	2.7	1.41	18	56	26	
Fine Fractions (<63 μm)									
15		422	7.2	25.5	1.40	15	74	11	
20		1169	6.6	38.3	1.22	8	86	6	
25		5217	1.6	1598	0.06			23	77
30		9357	1.6	2628	0.02			8	92
35		307	7.1	49.4	1.51	22	48	30	
40		215	7.2	30.7	2.17	43	30	27	

[a] Final pHs and total produced sulfate in the supernatants. Cumulative molar CO_2/O_2 ratios and sulfate production were used to calculate the relative contribution to the total O_2 consumption of the oxidation reactions (a−d, Table 1).

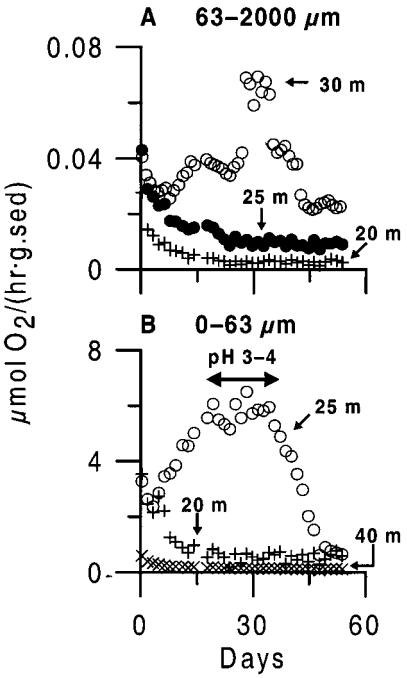

FIGURE 5. O_2 consumption rates during the incubation of coarse (A) and fine (B) fractions that dominantly showed unbuffered pyrite oxidation (○), buffered pyrite oxidation (●), SOM oxidation (+), or siderite oxidation (×). The rate maxima in O_2 consumption during unbuffered pyrite oxidation correspond with a modeled pH range of 3−4.

Pyrite. Buffered pyrite oxidation is the dominant (86%) oxygen-consuming process in the coarse fraction from 25 m (Figure 5a). Here, the O_2 consumption rates decreased continuously. Pyrite oxidation will result in the formation of iron hydroxides provided that the proton production is buffered by carbonate dissolution to keep the pH circumneutral. These iron hydroxides may precipitate on the pyrite surfaces and act as a diffusive resistance, slowing its oxidation (*44, 45*).

After the carbonate buffer had been consumed within 1 week of incubation, unbuffered pyrite oxidation started in the coarse (30 m, 75%) and fine (25 m, 77%) fractions (Figure 5a,b). During the acidification O_2 consumption rates started to increase up to a maximum, after which the rates dropped until the end of the experiments when the samples had acidified to a pH < 2. Since only the samples that showed unbuffered pyrite oxidation exhibit this typical sequence, we interpret this maximum in the O_2 consumption rate to be a pH effect. The pH-dependent dissolution of an inhibiting iron hydroxide coating, formed during buffered pyrite oxidation, and the subsequent production of ferric iron at acid pH, which is a rate-controlling intermediate in the oxidation of pyrite by O_2 (*46*), are probable causes for the increased rates compared with buffered pyrite oxidation. Furthermore, the modeled pH values of 2−4 during the maximum O_2 consumption rates approximate the reported optimal pH conditions for microbial ferrous iron oxidation (*47*). This suggests that bacteria, capable to facilitate acid pyrite oxidation, were already present in this initially reduced sediment. The final decrease in pyrite oxidation rates is probably due to the slow, rate-controlling, abiotic oxidation of ferrous iron at a pH < 2 (*37*).

Siderite. Although the quantification of low contents of siderite remains difficult, our CO_2/O_2 ratios indicate the importance of siderite as a reactive species in subsurface sediments. The fine fraction from 40 m depth showed the highest (43%) contribution by siderite oxidation (Table 2) and continuously decreasing O_2 consumption rates (Figure 5b). It also has the lowest total oxygen consumption of all incubated fine fractions, while the corresponding total fraction is relatively much more reactive. This suggests that the oxidation of siderite is a slower process, compared with the oxidation of pyrite or SOM. The chemical stability and weathering of siderite to form iron hydroxides in geological environments is well documented but rather little is known about the nature of siderite weathering itself (*48−50*). Similar to the inhibition during buffered pyrite oxidation, the iron oxyhydroxides coatings formed during siderite oxidation can potentially slow its oxidation.

Measured Reduction Capacity. Oxygen consumption of the sediment fractions slowed considerably during incubation but had not ended at the end of the incubations. Therefore, the total amount of O_2 consumption on a dry weight basis will be referred to as measured reduction capacity (mRC). The mRC of the total fractions (Table 2) was related to their geology and ranged from 8 μmol O_2/g in Kreftenheye Formation, to 20−84 μmol O_2/g in the Urk Formation. The mRCs of the sediments from the Sterksel Formation were intermediate (15−20 μmol O_2/g). This relative trend for the different formations is also reflected in the mRCs of the coarse (6−47 μmol O_2/g) and fine fractions (Table 2). This suggests that the reducing capacity of these sediments is related to their geological histories.

The mRCs of the fine fractions (Table 2) were around 2 orders of magnitude higher than those of the corresponding total fractions, due to the higher content of TOC (Figure 1) and associated diagenetic reductants in the fine fractions. However, the greater importance of the fine fraction in the Sterksel sediments (Figure 1) is not reflected by the intermediate mRCs of their total fractions. Moreover, the mRCs of the fine Sterksel fractions are lowest of all fine fractions. Probably, the differences in grain size distribution between the studied aquifer sands are too minor for the higher reduction capacity of the fine fraction to have profound effect on the reduction capacity of the total fractions. This is due to the fact that the significance of the fine fraction is relatively small in the total grain size distribution. Consequently, the coarse fraction mainly diluted the reduction activity of the fine fraction with its lowest overall mRC. This conclusion is in line with the lack of correlation found between the clay content and TRC of a sandy aquifer material (*26*).

Kinetic Controls on the Available Reduction Capacity. The mRCs after 54 days of incubation were around 10% of

the TRC calculated from pyrite and TOC contents of the carbonate buffered total fractions (Table 2). Thus, only a small fraction of the TRC present reacted during these incubations. As an exception, the mRC of the total fraction from 30 m depth was 42% of the calculated TRC. While SOM oxidation was suppressed at these low pHs, these results indicate that pH is an important factor controlling the oxidation rates of different reductants.

Previous studies on aquifer sediments used the standard method of acid dichromate oxidation (*26*, *27*) to measure reduction capacities. Using this method, Barcelona et al. (*22*, *51*) found the mRCs to be around 50% of the TRCs calculated from the total amounts of reduced solid species. While this indicates that still only a part of the TRC present in aquifer sediments is reactive at experimental time scales, this higher recovery is likely caused by the use of this abiotic method with a stronger oxidant under acid conditions that would promote pyrite oxidation. Furthermore, Pedersen et al. (*26*) found around 40% of the mRC remaining after having been exposed to oxygen and nitrate for about 2 years, in a study on an oxidation−reduction front in a shallow sandy aquifer using the same method.

Implications for Field Studies. Clearly, the reactivity of the subsurface reductants depends on the physicochemical conditions (oxidant type, temperature, pH) as well as on the intrinsic characteristics of the reductants that make up the TRC. For instance, the degradability of SOM is determined by its chemical composition and the strength of the degrading oxidant (*39*), while the occurrence of iron sulfide oxidation depends strongly on oxidant type and pH (*52*). Therefore, the mRC of subsurface sediments depends on the strength of the oxidant used and the applied conditions as well as on exposure time. Thus, while the use of the acid dichromate oxidation method may be appropriate in the context of an in-situ contaminant oxidation using Fenton's reagents, it is prone to overestimate the reduction capacity of aquifer sediments under milder conditions, since most redox reactions occurring in aquifers involve oxidation by weaker oxidants, such as oxygen, nitrate, ferric iron, sulfate, or tetrachloroethylene and are microbially mediated (*28*, *53*).

So far, studies did not address the contributions of various reductants (*22*, *26*, *27*, *51*). However, the secondary effects on groundwater quality may be quite different for the oxidation of SOM versus that of pyrite. For example the release of increased mobility of trace metals during pyrite oxidation (*54*, *55*) or the eutrophication by NH_4^+ or PO_4^- during SOM oxidation (*56*).

The reactivity of natural reductants is an important environmental issue, either during the natural attenuation of percolating nitrate or in competition with contaminants for injected oxidants. Our oxidation experiments with O_2 showed the simultaneous oxidation of reductants. Their relative contribution depends both on their relative amounts and their relative reactivity toward O_2. However, there is still limited knowledge about the controls on reactivity of characteristics such as the specific surface area of and coatings on pyrite (*45*) and the association and composition of SOM (*27*) on their reactivity of within aquifer sediments. Moreover, the reactivities of reductants present are affected by the conditions of the system to which they are exposed.

Incubations, which resulted in acidification, bear more resemblance to pyrite oxidation in leached topsoil. However, incubations under permanent carbonate buffering are relevant for many natural aquifer settings. Our buffered batch incubations show considerably lowered but still continuous oxygen consumption rates. Extrapolation of these rates, using an exponential decrease model, suggests that 20−40% of the TRC present in the sediments would remain after 2 years. While this estimate is in agreement with previous data (*26*), this is a crude estimate, since the calculated TRC does not account for contributions by reductants other than pyrite and SOM and assumes constant conditions.

In the field of reactive transport modeling, major uncertainties exist about the availability and reactivity of the solid redox-sensitive phases. Results of this study indicate that several reductants can be oxidized simultaneously and that their reactivities depend on both geological and environmental factors. These factors should be taken into account in order to describe and predict the development of groundwater chemistry. Moreover, considering the vertical heterogeneity in reduction activity in the studied aquifer, a reactive transport model would not only require model layering in its physical properties but in its geochemical reactivity as well (*57*).

Acknowledgments

The authors wish to thank Pim F. van Bergen for his comments and useful discussions that helped to improve this manuscript. This manuscript benefited from the comments of Pierre A. G. Regnier and two anonymous reviewers.

Supporting Information Available

Figure S1 of TGA-DTA measurements. This material is available free of charge via the Internet at http://pubs.acs.org.

Literature Cited

(1) Spalding, R. F.; Exner, M. E. *J. Environ. Qual.* **1993**, *22*, 392−402.
(2) Fraters, D.; Boumans, L. J. M.; van Drecht, G.; de Haan, T.; de Hoop, W. D. *Environ. Pollut.* **1998**, *102*, 479−485.
(3) Goodrich, J. A.; Lykins, J., B. W.; Clarck, R. M. *J. Environ. Qual.* **1991**, *20*, 707−717.
(4) Lin, B.-L.; Sakoda, A.; Shibasaki, R.; Suzuki, M. *Water Res.* **2001**, *35*, 1961−1968.
(5) Smith, R. L.; Duff, J. H. *Appl. Environ. Microbiol.* **1988**, *54*, 1071−1078.
(6) Postma, D.; Boesen, C.; Kristiansen, H.; Larsen, F. *Water Resour. Res.* **1991**, *27*, 2027−2045.
(7) Bradley, P. M.; Fernandez Jr, M.; Chapelle, F. H. *Environ. Sci. Technol.* **1992**, *28*, 2377−2381.
(8) Robertson, W. D.; Russell, B. M.; Cherry, J. A. *J. Hydrol.* **1996**, *180*, 267−281.
(9) Pauwels, H.; Kloppmann, W.; Foucher, J.-C.; Martelat, A.; Fritsche, V. *Appl. Geochem.* **1998**, *13*, 767−778.
(10) Pauwels, H.; Foucher, J.-C.; Kloppmann, W. *Chem. Geol.* **2000**, *168*, 307−324.
(11) Moncaster, S. J.; Botrell, S. H.; Tellam, J. H.; Lloyd, J. W.; Konhauser, K. O. *J. Contam. Hydrol.* **2000**, *43*, 147−163.
(12) Nielsen, P. H.; Albrechtsen, H.-J.; Heron, G.; Christensen, T. H. *J. Contam. Hydrol.* **1995**, *20*, 27−50.
(13) Nielsen, P. H.; Bjarnadóttir, H.; Winter, P. L.; Christensen, T. H. *J. Contam. Hydrol.* **1995**, *20*, 51−66.
(14) Nielsen, P. H.; Christensen, T. H. *J. Contam. Hydrol.* **1994**, *15*, 305−320.
(15) Nielsen, P. H.; Christensen, T. H. *J. Contam. Hydrol.* **1994**, *17*, 55−67.
(16) Coates, J. D.; Chakraborty, R.; Lack, J. G.; O'Connor, S. M.; Cole, K. A.; Bender, K. S.; Achenbach, L. A. *Nature* **2001**, *411*, 1039−1043.
(17) Lovely, D. R. *Biodegradation* **2000**, *11*, 107−116.
(18) Skubal, K. L.; Barcelona, M. J.; Adriaens, P. *J. Contam. Hydrol.* **2001**, *49*, 151−169.
(19) Bradley, P. M.; Chapelle, F. H.; Wilson, J. T. *J. Contam. Hydrol.* **1998**, *31*, 111−127.
(20) Cunningham, J. A.; Hopkins, G. D.; Lebron, C. A.; Reinhard, M. *Biodegradation* **2000**, *11*, 159−170.
(21) Baker, R. J.; Baehr, A. L.; Lahvis, M. A. *J. Contam. Hydrol.* **2000**, *41*, 175−192.
(22) Barcelona, M. J.; Holm, R. T. *Environ. Sci. Technol.* **1991**, *25*, 1565−1572.
(23) Appelo, C. A. J.; Postma, D. *Geochemistry, Groundwater Pollution*, 2nd ed.; Balkema: Rotterdam, 1993.
(24) Berner, R. A. *Principles of Chemical Sedimentology*; McGraw-Hill: New York, 1971.
(25) McMahon, P. B.; Chapelle, F. H. *Nature* **1991**, *349*, 233−235.
(26) Pedersen, J. K.; Bjerg, P. L.; Christensen, T. H. *J. Hydrol.* **1991**, *124*, 263−277.

(27) Christensen, T. H.; Bjerg, P. L.; Banwart, S. A.; Jakobsen, R.; Heron, G.; Albrechtsen, H.-J. *J. Contam. Hydrol.* **2000**, *45*, 165−241.
(28) Jakobsen, R.; Postma, D. *Geology* **1994**, *22*, 1103−1106.
(29) Parkhurst, D. L.; Appelo, C. A. J. *User's guide to PHREEQC (Version 2)*; U.S. Geological Survey, 1999.
(30) Borrego, A. G.; Prado, J. G.; Fuente, E.; Guillén, M. D.; Blanco, C. G. *J. Anal. Appl. Pyrolysis* **2000**, *56*, 1−21.
(31) Vassilev, S. V.; Vassileva, C. G. *Fuel Processing Technol.* **1996**, *48*, 85−106.
(32) Gotor, F. J.; Macías, M.; Ortega, A.; Criado, J. M. *Physics Chem. Minerals* **2000**, *27*, 495−503.
(33) Pankow, J. F. *Aquatic Chemistry Concepts*; Lewis Publishers: Boca Raton, London, New York, Washington, DC, 1991.
(34) Chapelle, F. H.; Bradley, P. M. *Geology* **1996**, *24*, 925−928.
(35) Sposito, G. *The Chemistry of Soils*; Oxford University Press: New York, 1989.
(36) Koretsky, C. *J. Hydrology* **2000**, *230*, 127−171.
(37) Stumm, W.; Morgan, J. J. *Aquatic Chemistry*; Wiley-Interscience: New York, 1970.
(38) Urban, N. R.; Ernst, K.; Bernasconi, S. *Geochim. Cosmochim. Acta* **1999**, *63*, 837−853.
(39) Kristensen, E.; Ahmed, S. I.; Devol, A. H. *Limnol. Oceanogr.* **1995**, *40*, 1430−1437.
(40) Cowie, G. L.; Hedges, J. I. *Nature* **1994**, *369*, 304−307.
(41) Hulthe, G.; Hulth, S.; Hall, P. O. J. *Geochim. Cosmochim. Acta* **1998**, *62*, 1319−1328.
(42) Mayer, L. M. *Chem. Geol.* **1994**, *114*, 347−363.
(43) Atlas, R. M.; Bartha, R. *Microbial Ecology: Fundamentals and Applications*, 4th ed.; Benjamin/Cummings Science Publishing: Menlo Park, CA, 1998.
(44) Nicholson, R. V.; Gillham, R. W.; Reardon, E. J. *Geochim. Cosmochim. Acta* **1990**, *54*, 395−402.
(45) Andersen, M. S.; Larsen, F.; Postma, D. *Environ. Sci. Technol.* **2001**, *35*, 4074−4079.
(46) Moses, C. O.; Herman, J. S. *Geochim. Cosmochim. Acta* **1991**, *55*, 471−482.
(47) Roychoudhury, A. N.; Violiler, E.; Van Cappellen, P. *Appl. Geochem.* **1998**, *13*, 269−280.
(48) Postma, D. *J. Soil Sci.* **1983**, *34*, 163−182.
(49) McMillan, S. G.; Schwertmann, U. *Eur. J. Soil Sci.* **1998**, *49*, 283−293.
(50) Weber, K. A.; Picardal, F. W.; Roden, E. E. *Environ. Sci. Technol.* **2001**, *35*, 1644−1650.
(51) Barcelona, M. J.; Holm, R. T. *Environ. Sci. Technol.* **1991**, *26*, 2540.
(52) Schippers, A.; Jørgensen, B. B. *Geochim. Cosmochim. Acta* **2002**, *66*, 85−92.
(53) Murphy, E. M.; Schramke, J. A.; Fredrickson, J. K.; Bledsoe, H. W.; Francis, A. J.; Sklarew, D. S.; Linehan, J. C. *Water Resour. Res.* **1992**, *28*, 723−740.
(54) Larsen, F.; Postma, D. *Environ. Sci. Technol.* **1997**, *31*, 2589−2595.
(55) Nickson, R. T.; McArthur, J. M.; Ravenscroft, P.; Burgess, W. G.; Ahmed, K. M. *Appl. Geochem.* **2000**, *15*, 403−413.
(56) Nolan, B. T.; Stoner, J. D. *Environ. Sci. Technol.* **2000**, *34*, 1156−1165.
(57) Islam, J.; Singhal, N.; O'Sullivan, M. *Transport Porous Media* **2001**, *43*, 407−440.

Received for review September 5, 2001. Revised manuscript received April 4, 2002. Accepted April 8, 2002.

ES015681S

Supporting Information

Corresponding to manuscript "Distribution and reactivity of O_2-reducing components in sediments from a layered aquifer" by N. Hartog, J. Griffioen and C.H. van der Weijden. Submitted to Environmental Science & Technology.

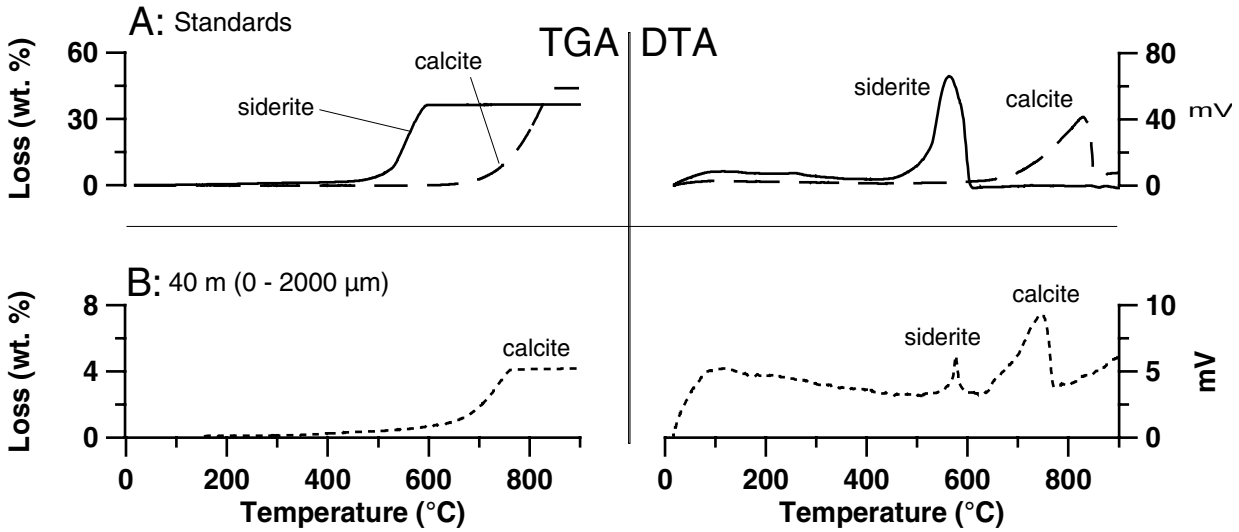

FIGURE S1

FIGURE S1. A: -TGA-DTA measurements (N_2-atmosphere/5°C.min-1 to 900°C on a Setaram TG-DTA92) A: TGA of ($FeCO_3$) and calcite ($CaCO_3$) standards and 0-2 mm fraction from 40 meters deep. B: DTA of ($FeCO_3$) and calcite ($CaCO_3$) standards and 0-2 mm fraction from 40 meters deep.

Erratum

Corresponding to Hartog, N., J. Griffioen, and C.H. Van Der Weijden (2002) "Distribution and reactivity of O2-reducing components in sediments from a layered aquifer" Environmental Science and Technology, 36(11), 2436-2442

Apologies for any inconvenience caused.

August 6th,2009 – It has come to my attention that a spreadsheet error has unfortunately caused incorrect values in **Table 2**, as originally published for the samples that showed unbuffered pyrite oxidation. Below are the corrected relative contribution (**in bold)** to the total O_2 consumption of the oxidation reactions (a-d, Table 1).

Depth	TRC	mRC	pH	SO_4	CO_2/O_2	**Oxidation reactions (%)**			
(m)	(µmol O_2/g)	(µmol O_2/g)		(µmol/ g)	(molar)	(a)	(b)	(c)	(d)
			Total Fractions (0–2 mm)						
30	199	84	2.1	19.1	0.02			**4**	**96**
			Fine Fractions (< 63 µm)						
25		5217	1.6	1598	0.06			**11**	**89**
30		9357	1.6	2628	0.02			**4**	**96**

$f_{pyr-unbuf}$ (d) is calculated using eq 5, where $\sum O_2{}^*$ is the total amount of oxygen consumption that was unaccompanied by CO_2 release using $f_{pyr-unbuf} = \frac{\sum O_2{}^*}{\sum O_2}$ (Equation 5) (which equals

$$f_{pyr-unbuf} = 1 - f_{pyr-buf} = 1 - \frac{15\sum CO_2}{8\sum O_2})$$

Dr. Niels Hartog